https://doi.org/10.5194/egusphere-2026-3338
Preprint. Discussion started: 5 August 2026

Radiocarbon-based source apportionment of carbonaceous aerosols over the Athabasca Oil Sands Region in Alberta, Canada

Lurui Niu[1], Xiaomei Xu[1], Elizabeth B. Wiggins[1], James T. Randerson[1], Allison M. Welch[1], Guaciara D. Santos[1], Rebecca J. Sheesley[2], Claire E. Moffett[2], Claudia I. Czimczik[1]

[1]Department of Earth System Science, University of California, Irvine, CA, USA
[2]Department of Environmental Science, Baylor University, Waco, TX, USA

Correspondence to: Lurui Niu (luruin1@uci.edu) and Claudia Czimczik (czimczik@uci.edu)

Abstract

The Athabasca Oil Sands Region (AOSR) hosts one of the world's largest unconventional fossil fuel operations, producing a complex carbonaceous aerosol mixture: fossil emissions from oil sands operations, biogenic secondary organic aerosol (SOA) from surrounding boreal landscapes, and episodic wildfire emissions, with consequences for regional air quality and climate. Here, we present a first dual-isotope ($^{14}C/\delta^{13}C$) source apportionment of total carbon (TC) and elemental carbon (EC) in $PM_{2.5}$ collected at Fort McKay from May to October 2017. Sampling-day $PM_{2.5}$ ranged 0.8-20.3 μg m^{-3} (mean 6.9 ± 4.7, n = 29), versus 0.2-38.1 μg m^{-3} in the continuous record, indicating that filter sampling did not capture the highest pollution episodes. TC and organic carbon (OC) correlated strongly (Spearman ρ = 0.89) and positively with temperature (ρ = 0.67), consistent with biogenic SOA. EC co-varied with NO_2 (ρ = 0.77) and SO_2 (ρ = 0.51), implicating diesel mining fleets and upgrader stacks. During smoke-free periods, fossil fuel combustion dominated TC (mean: 51%, range: 26-77%), with westerly air masses crossing active mining areas more ^{14}C-depleted ($F^{14}C$ = 0.58 ± 0.22) than northerly masses ($F^{14}C$ = 0.63 ± 0.14). During wildfire-impacted periods, biomass burning was the dominant source (f_{bb} mean: 45%, range: 9-76%). The AOSR exhibited substantially lower summertime $F^{14}C$ values than Arctic and boreal comparison sites during non-fire periods, reflecting persistent local fossil fuel influence. These results provide information that can contribute to an isotopic baseline for emission inventories, atmospheric models, and air quality management in the AOSR.

https://doi.org/10.5194/egusphere-2026-3338
Preprint. Discussion started: 5 August 2026

1 Introduction

Oil sands, classified as a non-conventional fuel reserve, are an unconsolidated mixture of sand, clay, water, and bitumen, an extra-heavy, viscous crude oil. The largest oil sand deposits are in Alberta, Canada (174.5 billion barrels), accounting for 70% of global resources (Hein, 2006). Major developed oil sands reservoirs are the Athabasca (93,000 km^2), Peace River (29,000 km^2), and Cold Lake (18,000 km^2) deposits (OSMP, 2025), of which Athabasca is the only deposit shallow enough for surface mining (Berkowitz and Speight, 1975).

Bitumen extraction from oil sands is a land-, water-, and energy-intensive process that generates substantial atmospheric emissions (Liggio et al., 2019; Rosa et al., 2017; Wang et al., 2023). Approximately 20% of Alberta's reserves lie within 50-70 m of the surface and are accessible by open-pit mining. During surface mining, large volumes of overburden and oil sands ore are transported by diesel-powered heavy-haul truck to bitumen extraction facilities, where crushing and hot-water extraction are used to separate bitumen from mineral material. These operations produce fugitive dust from haul roads and tailings deposits, as well as combustion emissions from heavy-duty diesel machinery. Open-pit mining also generates large quantities of fluid fine tailings (20-30 wt% fine particles in water) that mature into gel-like suspensions and can act as ongoing sources of particulate matter through wind-driven resuspension.

Most bitumen reserves occur at depths greater than 200 m and are extracted using *in situ* techniques, which involve steam injection to mobilize bitumen for recovery. Unlike surface mining, *in situ* extraction does not produce large tailings areas, but requires substantially more energy input, resulting in higher combustion-related emissions per barrel from steam generation boilers and associated upgrading operations. Following extraction by either method, bitumen is upgraded into synthetic crude oil, or the bitumen is diluted with natural gas condensate to enable pipeline transport to refineries. These upgrading and transport preparation steps are associated with additional emissions of nitrogen oxides (NO_x), sulphur dioxide (SO_2), and carbonaceous particulate matter from upgrader stacks and flaring (Gordon et al., 2015; Horb et al., 2021). Together, surface mining operations, *in situ* extraction, and bitumen upgrading represent the principal local sources of primary combustion emissions and fugitive dust within the Athabasca Oil Sands Region (AOSR) (Horb et al., 2021; Rosa et al., 2017).

In addition to its contributions of greenhouse gas emissions, primarily CO_2 from fuel combustion and upgrading (Horb et al., 2021; Liggio et al., 2019; McGaughy et al., 2025), and its impacts land and freshwater resources (Arciszewski et al., 2021; Jordaan, 2012), Alberta's oil sand industry is a significant source of atmospheric pollutants that degrade regional air quality (Bari and Kindzierski, 2015, 2017; Horb et al., 2021). Oil sands activities emit substantial quantities of particulate matter (PM), nitrogen oxides (NO_x = NO + NO_2), SO_2, volatile organic compounds (VOCs), ozone (O_3), nitric acid, ammonia, polycyclic aromatic compounds, reduced sulphur compounds (including H_2S), and mercury (Horb et al., 2021). Off-road mining fleets (diesel heavy haulers and shovels) together with upgrader and flaring stacks are the principal sources of NO_x, while upgrader stacks are also major sources of SO_2 (Gordon et al., 2015; Horb et al., 2021; McLinden et al., 2014, 2016; Zhang et al., 2015) and gaseous organic compounds (He et al., 2024). The Oil Sands Monitoring Program, jointly managed by the governments of Canada and Alberta with participation of Indigenous communities since 2012, has documented that regional air quality is generally good and has been improving over time. Locally and intermittently, however, Alberta's Ambient Air Quality Objectives/Guidelines at permanent monitoring stations are being exceeded for dust (total suspended particles), fine particulate matter ($PM_{2.5}$), H_2S, O_3, and SO_2 (Oil Sands Monitoring Program, 2025). $PM_{2.5}$ is of particular concern due to its adverse impacts on human health, including cardiopulmonary disease and premature mortality, as well as its role in climate forcing (Fuzzi et al., 2015). A substantial fraction

https://doi.org/10.5194/egusphere-2026-3338
Preprint. Discussion started: 5 August 2026

of $PM_{2.5}$ mass consists of carbonaceous aerosols, comprising organic carbon (OC) and elemental carbon (EC, closely related to optically-defined black carbon), which affect both air quality and radiative forcing, with EC being a potent short-lived climate forcer (Bond et al., 2013). In the AOSR, where $PM_{2.5}$ originates from a complex mixture of sources, quantifying the carbonaceous fraction and distinguishing its sources is particularly important for understanding the overall $PM_{2.5}$ burden and its climate implications.

While dust generated during surface mining is the dominant source (83-95% of total mass) of coarse particle mass ($PM_{10-2.5}$) in the AOSR (Horb et al., 2021), sources of fine particulate matter ($PM_{2.5}$) are less well understood and more variable. Ground- and aircraft observations, combined with receptor modelling (Landis et al., 2017; Phillips-Smith et al., 2017; Xing et al., 2020) indicate that $PM_{2.5}$ contributions arise from mineral matter including fugitive dust from haul road and tailing area (30-60%), emissions from upgrader and flaring stacks (20-60%), biomass burning (0-26%), and long-range transport (<10%). Collectively, these results suggest that oil sands mining, upgrading, and associated heavy transportation fleets are significant contributors to ambient aerosol concentrations within the AOSR, yet the specific partitioning between fossil combustion and contemporary carbon sources remains poorly constrained by existing chemical mass balance and receptor modelling approaches.

Quantifying the contributions of oil sands activities to $PM_{2.5}$ in the AOSR is further complicated by the presence of multiple natural and anthropogenic sources, since $PM_{2.5}$ persists in the atmosphere for days to weeks. Biogenic VOC emissions from boreal vegetation can be a major source of secondary organic aerosol (Spracklen et al., 2008; Wang et al., 2024), and frequent wildfires (Scholten et al., 2024) drive short-term extremes in $PM_{2.5}$ concentrations (Landis et al., 2018; Mouteva et al., 2017; Welch et al., 2025). Urban areas and agriculture are additional sources of primary and secondary aerosol (Landis et al., 2017; You et al., 2024).

Isotopic analysis of carbonaceous aerosol, including radiocarbon (^{14}C) and stable isotope ($\delta^{13}C$) measurements, has emerged as a powerful tool for distinguishing fossil fuel contributions from biogenic sources in the Arctic and boreal regions (e.g., Moffett et al., 2022; Mouteva et al., 2015a; Welch et al., 2025; Winiger et al., 2017, 2019). This isotopic approach provides a direct, quantitative distinction between fossil (^{14}C-depleted) and contemporary biogenic (^{14}C-modern) carbon sources that is independent of air mass back-trajectories and emission inventories, which can be highly uncertain in complex source regions. While previous source apportionment studies, including chemical mass balance analyses by Landis et al. (2017) and receptor modelling by Phillips-Smith et al. (2017), have characterised $PM_{2.5}$ composition and source contributions in the AOSR, direct quantification of fossil versus contemporary carbon using radiocarbon analysis has not previously been conducted in this region.

Fort McKay, located approximately 60 km north of Fort McMurray and surrounded by active mining and upgrading facilities, represents a receptor site directly influenced by oil sands operations while also experiencing regional biogenic and wildfire emissions. Here, we combine weekly measurements of the isotopic composition (^{14}C /^{12}C and ^{13}C /^{12}C) of $PM_{2.5}$ in Fort McKay from May to October 2017 with continually monitored air pollutants to assess the impact of oil sands operations and contemporary carbon sources from vegetation and wildfires on air quality in the AOSR. The 2017 sampling period occurred one year after the 2016 Horse River Fire, which burned approximately 590 kha (Landis et al., 2018) and temporarily reduced oil sands production. While 2017 was a relatively low fire year in Alberta (47 kha burned), it was a high fire year for Canada overall, with 3.46 Mha burned primarily due to extensive fires in British Columbia (CIFFC, 2018).

Specifically, the study addresses the following research questions: (1) What are the seasonal dynamics of the concentration and composition of $PM_{2.5}$ and carbonaceous aerosol?, (2) How much do fossil and non-fossil sources contribute to the concentration and composition of $PM_{2.5}$?, and (3) How do $PM_{2.5}$ concentrations and sources compare to other parts of the North American Arctic and boreal regions? Together, this study provides one of the first characterizations of the isotopic composition of carbonaceous

https://doi.org/10.5194/egusphere-2026-3338
Preprint. Discussion started: 5 August 2026

$PM_{2.5}$ in the AOSR, enabling improved source apportionment that can inform evidence-based air quality management as oil sands operations and climate-driven wildfire activity evolve.

2 Materials and Methods

2.1 Site and Aerosol Sampling

2.1.1 Regional Municipality of Wood Buffalo

The Wood Buffalo Environmental Association (WBEA) Bertha Ganter-Fort McKay (AMS 1) ambient air monitoring station (57.189428, -111.640583; NAPS ID: 90801) is in the Fort McKay First Nation and Metis community, Alberta, Canada. This station is located within 5 km of several active surface oil sand operations that include mining and bitumen upgrading and was selected as the sampling site for this project.

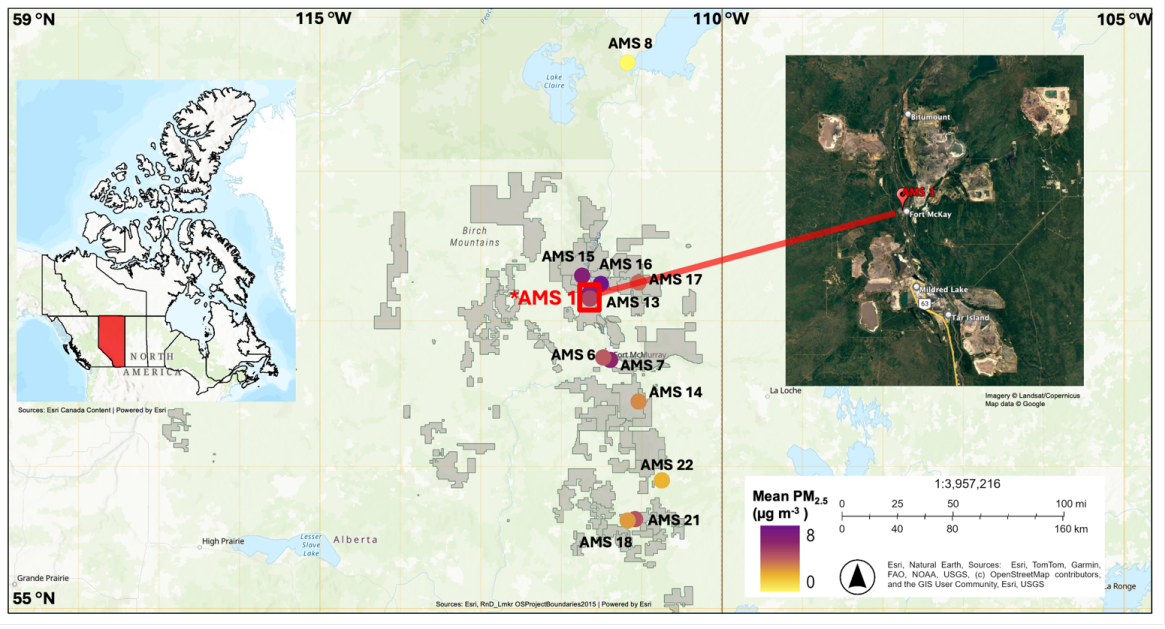

Figure 1. Study area and locations of the Wood Buffalo Environmental Association (WBEA) monitoring stations within the Athabasca Oil Sands Region, Alberta, Canada. The main map shows the oil sands deposit areas (grey polygons outlined in green) and the WBEA monitoring stations. Circle colors represent the mean $PM_{2.5}$ concentrations (µg m^{-3}) measured at the 12 WBEA monitoring sites between May and October 2017. The map on the left shows the location of Alberta, Canada. The Google Earth image on the right shows the location of Bertha Ganter-Fort McKay ambient air monitoring station (AMS 1) in Alberta, where aerosol samples and isotope measurements were collected. Map attribution: Left inset: Sources: Esri Canada Content | Powered by Esri. Main map: Sources: Esri, RnD_Lmkr OSProjectBoundaries2015 | Powered by Esri. Right inset: Imagery © Landsat/Copernicus; Map data © Google.

https://doi.org/10.5194/egusphere-2026-3338
Preprint. Discussion started: 5 August 2026

A total of 29 $PM_{2.5}$ aerosol samples were collected weekly from May to October 2017, with each sampling event lasting 24 h. Sampling was conducted using a high-volume total suspended particulate sampler (HIVOL-AMCLD, Thermo Environmental Instruments) equipped with $PM_{2.5}$ impactor plates (TE-230-QZ, Tisch Environmental) and operated at a flow rate of 40 cfm (67.9 $m^3\ h^{-1}$). Samples were collected on pre-baked (500°C for 4 h) quartz microfiber filters (20 cm × 25 cm, 2500 QAT-UP, Pallflex Tissuquartz, Pall Corporation). All collection filters were wrapped in pre-baked aluminium foil and stored in sealed polyethylene bags. A slotted micro-quartz fibre filter (TE-230-QZ, Tisch) was placed in the impactor head during each sampling period to remove coarse particles (>2.5 µm). These impactor filters served solely for size separation and discarded after each sampling event. Field blank filters (one-fourth of a pre-baked collection filter) were mounted inside the sampler housing without exposure to air flow. Following the 24 h sampling period, filters remained in the sampler until the next scheduled sampling event. During collection, sample and blank filters were removed from the sampler, wrapped in pre-baked aluminium foil, sealed in polyethylene bags, and stored at -20°C on-site until transport to the University of California, Irvine (UCI) with ice packs, and then stored at -20°C again until analysis. Storing sample filters at -20°C immediately after collection and maintaining the cold chain throughout transport minimises post-sampling evaporative loss of semi-volatile organic compounds and biological degradation of carbonaceous material.

In addition to aerosol sampling, air quality was continuously monitored throughout the study period at station AMS 1 and 11 additional stations across the Regional Municipality of Wood Buffalo (Table S1). Measurements included daily concentrations of $PM_{2.5}$, NO_2, NO_x, SO_2, and O_3 (for details see Text S1).

2.1.2 Arctic Comparison Sites

To place the AOSR results in a broader regional context, we compared the isotopic composition of $PM_{2.5}$ collected at AMS 1 with carbonaceous aerosol measurements from previous studies at Arctic and boreal sites across North America (Table 1).

Table 1. North American Arctic and boreal sites with radiocarbon (^{14}C) measurements of carbonaceous aerosol.

Site	Location (°N, °W)	Region	Sampling period	Species	Source
AMS 1, NAPS ID: 90801	57.19, 111.64	Boreal / Athabasca Oil Sands Region (Alberta, Canada)	2017-05-07 – 2017-10-28	$PM_{2.5}$	this study
Caribou Poker Creek Long-Term Ecological Research Station	65.13, 147.45	Boreal (interior Alaska, USA)	2013-06-27 – 2013-08-08	$PM_{2.5}$	Mouteva et al. 2015b
Delta Junction Agricultural & Forestry Experimental Site	63.97, 145.40		2013-06-28 – 2013-08-10	$PM_{2.5}$	Mouteva et al. 2015b
Toolik Field Station	68.63, 149.60	Arctic (interior, North Slope, AK)	2022-06-21 – 2022-08-30 2023-06-19 – 2023-08-05	TSP	Welch et al. 2025
			2012-07-16 to 2013-06-04	PM_{10}	Barrett and Sheesley 2017,
Utqiaġvik	71.29, 156.79	Arctic (coastal, North Slope, AK)	2015-08-24 – 2015-09-28 2016-06-14 to 2017-08-30	TSP	Winiger et al. 2019 Moffett et al. 2020*
			2022-07-20 – 2022-09-01 2023-06-23 to 2023-08-12	TSP	Welch et al. 2025
Oliktok Point	70.50, 149.89	Arctic / oil field (coastal, North Slope, AK)	2015-08-18 – 2015-10-05 2016-06-15 to 2017-09-13	TSP	Moffett et al., 2020, Moffett et al. 2022*

https://doi.org/10.5194/egusphere-2026-3338
Preprint. Discussion started: 5 August 2026

*$\delta^{13}C$ data not previously reported.

135

2.2 Laboratory Analyses

2.2.1 Organic and Elemental Carbon

OC and EC mass concentrations (μg C cm^{-2}) were quantified from 1.5 cm^2 filter punches (SP-15, Sunset) using the NIOSH 5040 thermal-optical transmittance (TOT) method (Birch and Cary, 1996) on a Sunset Laboratory carbon analyser. The NIOSH 5040
140 protocol was selected because it is the standard method used across North American $PM_{2.5}$ monitoring networks, facilitating direct comparison with long-term WBEA monitoring data, and because its TOT charring correction minimises pyrolysis artefacts during the high-temperature oxidation steps. Measurements were corrected using instrument blanks and calibrated with sucrose standards. Field blanks were processed identically; their OC and EC values were averaged by sampling month and subtracted from sample values. OC and EC concentrations (ng C m^{-3}) were calculated from the measured filter loadings, sampling flow rate, sampling
145 duration, and filter punch area. Total carbon (TC) was calculated as the sum of the OC and EC concentrations.

2.2.2 Bulk Elemental and Stable Isotope Analyses

Bulk aerosol carbon content (%C), nitrogen content (%N), and stable isotope ratios ($\delta^{13}C$ and $\delta^{15}N$) were determined from two 1.5 cm^2 filter punches per sample. They were placed in tin capsules (5 mm × 9 mm, 041077, Costech Analytical Technologies) and analysed using an elemental analyser (EA; Fisons NA-1500NC, Thermo Fisher Scientific) coupled to an isotope-ratio mass
150 spectrometer (IRMS; DeltaPlus XL, Thermo Fisher Scientific) at UCI's W.M. Keck Carbon Cycle Accelerator Mass Spectrometry (KCCAMS) facility. Samples were analysed alongside field blanks and analytical standards. Isotope ratios are reported in conventional δ notation (‰) (Eq.1):

$$\delta(\%) = \left[\left(\frac{R_{sample}}{R_{standard}}\right) - 1\right] \times 1000 \qquad (1)$$

where R is the $^{13}C/^{12}C$ or $^{15}N/^{14}N$ isotope ratio of the sample or standard, respectively. $\delta^{13}C$ values are reported relative to the
155 Vienna Pee Dee Belemnite (VPDB) international standard, and $\delta^{15}N$ values relative to atmospheric N_2 (AIR). Blank corrections were applied using field blanks. Measurement precision, based on long-term analyses at the UCI KCCAMS facility, was ±0.2‰ (1σ) for both $\delta^{13}C$ and $\delta^{15}N$.

To assess whether mineral carbonate dust from oil sands mining operations contributed inorganic carbon to the aerosol filters, which would bias $\delta^{13}C$ and TC measurements, eight samples spanning the range of observed $PM_{2.5}$ loadings were subjected to acid
160 fumigation pre-treatment. Two 1.5 cm^2 punches per sample were placed in silver capsules (6 mm × 6 mm × 12 mm, Elementar) and exposed to concentrated hydrochloric acid vapour (37%, Merck) in a glass desiccator heated to 80°C for 1 h to volatilise carbonates (Jankowski et al., 2008). After fumigation, samples were transferred to a clean fume hood to allow residual acid to dissipate, then analysed for %C, %N, $\delta^{13}C$, and $\delta^{15}N$ as described above. Acid fumigation produced negligible changes in $\delta^{13}C$, ruling out carbonate carbon from fugitive mine dust as a contributor to bulk $\delta^{13}C$ variability; no carbonate correction was therefore
165 applied to the remaining samples.

https://doi.org/10.5194/egusphere-2026-3338
Preprint. Discussion started: 5 August 2026

2.2.3 Radiocarbon Analysis

For ^{14}C measurements of TC, multiple 1.5 cm^2 filter punches were sealed under vacuum in pre-combusted quartz tubes (9 mm o.d.) with 80-100 mg CuO and combusted at 900°C for 3 h. The resulting CO_2 was cryogenically purified on a vacuum extraction line, quantified manometrically (reported as µg C), sealed in a pre-combusted Pyrex reaction tube with catalysts (Zn, TiH_2, and Fe), and reduced to graphite using a sealed-tube zinc reduction technique (Xu et al., 2007). TC concentrations (ng C m^{-3}) were calculated from sampling flow rate, duration, number of filter punches, and filter area.

The two samples with the highest TC concentrations were additionally analysed for ^{14}C in EC. Following removal of water-soluble OC, EC was isolated and combusted to CO_2 using the Swiss_4S protocol on a Sunset Laboratory OC/EC analyser equipped with a non-dispersive infrared detector (NDIR) (Mouteva et al., 2015a). The EC-derived CO_2 isolated from three 1.5 cm^2 punches per sample was combined on a vacuum line, sealed in Pyrex reaction tubes (6 mm o.d.) containing Zn and Fe catalysts, and converted to graphite using a modified sealed-tube zinc reduction method optimized for ultra-small samples (Walker and Xu, 2019).

Graphite samples were analysed alongside graphitization standards (OX1, NIST SRM 4990B; OX2, NIST SRM 4990C) and procedural blanks using accelerator mass spectrometry (AMS; 1.5SDH-1, National Electrostatics Corporation) at the KCCAMS facility (Beverly et al., 2010). Data were corrected for field and processing blanks and reported as fraction modern carbon (referred to as $F^{14}C$ or Fraction Modern), with an analytical uncertainty of 2-3‰ (1σ) for modern samples, based on long-term measurements of secondary standards. $F^{14}C$ expresses the $^{14}C/^{12}C$ ratio of a sample, normalized to a $\delta^{13}C$ value of -25‰, relative to 0.95 times the $^{14}C/^{12}C$ ratio of the primary standard OX1 (NIST SRM 4990B) with a $\delta^{13}C$ value of -19‰ (Eq. 2):

$$F^{14}C = \frac{\frac{^{14}C}{^{12}C}_{sample\_-25}}{0.95\,\frac{^{14}C}{^{12}C}_{OX1\_-19}} \quad (2)$$

2.3 Data Analyses

2.3.1 Air Mass Back-Trajectories and Wildfire Smoke Identification

To identify source regions of collected aerosols, 10-day air mass back-trajectories were calculated for the AMS 1 station using the NOAA Hybrid Single-Particle Lagrangian Integrated Trajectory (HYSPLIT) model (version 5.2.0, January 2022; Rolph et al., 2017; Stein et al., 2015), driven by meteorological data from NOAA's Global Data Assimilation System (GDAS, 1° resolution). For each sampling period, trajectories were computed at 6 h intervals over a 240 h (10-day) backward window, starting at 270 m above ground level (agl) and with a model top at 10,000 m agl. Distinct transport patterns were identified using the HYSPLIT clustering algorithm, which iteratively merges trajectory pairs until a substantial increase in total spatial variance (TSV) is detected. Resulting clusters were exported and visualised (Fig. S1-3). Sampling periods affected by wildfire smoke at AMS 1 and along the back-trajectory paths were identified using NOAA's Hazard Mapping System (HMS) Fire and Smoke Product.

2.3.2 Aerosol Source Apportionment

Radiocarbon data were used to apportion TC and EC between fossil and non-fossil (contemporary) sources. For smoke-free periods, a two-source isotopic mass balance was applied (Eqs. 3–4):

$$f_c + f_{ff} = 1 \quad (3)$$

$$F^{14}C_{spl} = F^{14}C_{ff} f_{ff} + F^{14}C_c (1 - f_{ff}) \quad (4)$$

https://doi.org/10.5194/egusphere-2026-3338
Preprint. Discussion started: 5 August 2026

where f_c and f_{ff} are the fractional contributions of contemporary and fossil fuel sources to TC (or EC) mass, and $F^{14}C$ is the Fraction Modern of the sample (spl) or its respective source. A mean atmospheric $F^{14}C_c = 1.01 \pm 0.00$ (n = 38) was adopted from $^{14}CO_2$ measurements at Point Barrow, AK, USA, for May - October 2017 (X. Xu, personal communication, 2019). $F^{14}C_{ff} = 0$ because ^{14}C decays with a half-life of 5,730 years, rendering fossil carbon ^{14}C-depleted.

For smoke-impacted periods, a three-source dual-isotope Monte Carlo (MC) simulation was applied (Fang et al., 2018, 2023; Jiang et al., 2022), solving the following system (Eq. 5):

$$\begin{pmatrix} F^{14}C_{spl} \\ d^{13}C_{spl} \\ 1 \end{pmatrix} = \begin{pmatrix} F^{14}C_{bb} & F^{14}C_{ff} & F^{14}C_c \\ d^{13}C_{bb} & d^{13}C_{ff} & d^{13}C_c \\ 1 & 1 & 1 \end{pmatrix} \cdot \begin{pmatrix} f_{bb} \\ f_{ff} \\ f_c \end{pmatrix} \quad (5)$$

where f_{bb}, f_{ff}, and f_c denote the fractional contributions from biomass burning, fossil fuel combustion, and contemporary biogenic emissions, respectively, subject to the constraint $f_{bb} + f_{ff} + f_c = 1$. Source endmember values were represented as Gaussian probability density functions (PDFs) with means and standard deviations (1σ) derived from the literature: boreal wildfire biomass burning ($F^{14}_{bb} = 1.11 \pm 0.02$, $\delta^{13}C_{bb} = -27.2 \pm 0.2$‰; Mouteva et al., 2015b), fossil fuel combustion ($F^{14}C_{ff} = 0$, $\delta^{13}C_{ff} = -24.9 \pm 3.1$‰; Martinsson et al., 2017), and contemporary biogenic emissions ($F^{14}C_c = 1.01 \pm 0.00$; X. Xu personal communication, 2019; $\delta^{13}C_c = -27.17 \pm 1.56$‰; Martinsson et al., 2017). The MC simulation was performed using the measured $F^{14}C$ and $\delta^{13}C$ values for each sample together with the source endmember distributions and Eq. 5, with 100,000 iterations per sample. Each iteration drew independent random values for all isotopic inputs from their respective Gaussian distributions and solved the linear system analytically for f_{bb}, f_{ff}, and f_c. Iterations yielding negative fractions or fractions exceeding unity were rejected, and the reported source contributions represent the mean of the retained iterations (Table S4).

A key limitation of the dual-isotope Monte Carlo approach applied here concerns the separation of boreal wildfire biomass burning (bb) and contemporary biogenic (c) source contributions. The two endmembers have nearly identical $\delta^{13}C$ signatures, and the sole isotopic lever separating them is the difference in $F^{14}C$, a separation of only 0.10 $F^{14}C$ units. While this difference is real and analytically resolvable in individual measurements, it is modest relative to the propagated uncertainty across 100,000 Monte Carlo iterations that simultaneously randomize all six endmember parameters and both measured isotopic values. The consequence is visible in the wide credible intervals for f_{bb} and f_c during smoke-impacted periods (Table S4): the 90% credible intervals for these two fractions frequently span 0.6-0.8 units, and the number of physically retained iterations drops substantially for several samples, indicating that most random endmember realizations produce isotopically inconsistent solutions. We therefore caution that the individual f_{bb} and f_c values reported for smoke-impacted samples carry large and asymmetric uncertainties. Future work incorporating additional tracers capable of distinguishing pyrogenic from biogenic organic carbon, such as levoglucosan-to-OC ratios, would substantially reduce uncertainty in the biomass burning vs. contemporary biogenic source partitioning during fire-influenced periods.

2.4 Statistical Analyses

Spearman rank correlation (ρ) was used to evaluate monotonic relationships between carbonaceous aerosol components (TC, OC, EC) and meteorological variables (temperature, relative humidity, wind speed) and co-emitted trace gases ($PM_{2.5}$, O_3, NO_2, SO_2). Spearman ρ was preferred over Pearson *r* given the small sample size ($n = 29$) and the expected non-normal distributions of aerosol concentrations across background and smoke-impacted periods. To control the family-wise Type I error rate, a Bonferroni correction was applied separately within each correlation group, with the adjusted significance threshold defined as $\alpha^* = 0.05/k$,

https://doi.org/10.5194/egusphere-2026-3338
Preprint. Discussion started: 5 August 2026

where k is the number of correlations tested within that group. Spearman ρ was computed on all 29 samples; smoke-impacted (n = 17) and smoke-free (n = 12) periods are distinguished by color in scatter plots to illustrate source-specific patterns, but subgroup sample sizes are insufficient for separate hypothesis testing (Fig. S2a-S2c). All analyses were performed in Python using Jupyter notebook. Correlations with $p < \alpha^*$ are considered statistically significant.

3 Results and Discussion

3.1 Spatial Variability in $PM_{2.5}$ Across the AOSR Monitoring Network

Mean daily $PM_{2.5}$ concentrations varied substantially across the 12 WBEA monitoring stations in the Regional Municipality of Wood Buffalo between 1 May and 31 October 2017 (Fig. 1). The lowest mean $PM_{2.5}$ concentrations (3.8 µg m^{-3}) were recorded at AMS 8, the northernmost station situated within an environmentally protected boreal forest, while the highest values were observed at AMS 1, AMS 15, and AMS 16 (6.9, 7.1, and 7.8 µg m^{-3}, respectively), all located near Fort McKay in close proximity to active oil sands mining and upgrading facilities.

The spatial distribution revealed a distinct concentration hotspot centred near Fort McKay, with values decreasing progressively toward the south and southeast. This north-south elongation of elevated concentrations was consistent with channelled air mass transport along the Athabasca River Valley, which preferentially enhances pollutant dispersion in the north-south direction relative to east-west (Horb et al., 2021). Fort McKay lies within 5 km of several active surface mining and bitumen upgrading facilities, and the observed spatial gradient likely reflects the combined influence of proximity to these oil sands emission sources and topographic channelling that concentrates and directs these emissions along the valley corridor. Overall, these results indicate that $PM_{2.5}$ in this region is strongly controlled by proximity to industrial emission sources (oil sand operation) and local topographic channelling, with clear spatial gradients apparent across the monitoring network.

3.2 Air Quality at AMS 1

3.2.1 Temporal Variability in $PM_{2.5}$ and Carbonaceous Aerosol Concentrations

Our sampling approach captured a diverse range of air source regions and atmospheric conditions at WBEA AMS 1 station (Fig. S1a-S1c). Continuous $PM_{2.5}$ monitoring at AMS 1 yielded a mean daily concentration of 6.9 ± 4.8 µg m^{-3} over the full study period (1 May-31 October 2017), with a daily range of 0.2 to 38.1 µg m^{-3} (Fig. 2, Table S1). On the 29 days during which a 24 h $PM_{2.5}$ filter sample was collected for isotopic analysis, the corresponding subset of routine-monitor $PM_{2.5}$ ranged from 0.8 to 20.3 µg m^{-3} (mean 6.9 ± 4.7 µg m^{-3}; Table S2). Filter sampling therefore reflects typical warm-season conditions at AMS 1 but did not coincide with the highest pollution episodes captured by the continuous record. Air quality was classified as "Good" on most days according to U.S. EPA criteria (EPA, 2003) but reached the "Moderate" threshold (>12 µg m^{-3}) on six days, with a daily maximum of 38.1 µg m^{-3} recorded on 31 May 2017 (which coincided with one of the filter samples). These continuous-monitoring data are in good agreement with the long-term mean of 6.8 ± 12.9 µg m^{-3} recorded at the same station between 1999 and 2015 (Landis et al., 2017), indicating that 2017 was broadly representative of typical warm-season conditions at this site.

TC concentrations, measured by sealed-tube combustion on a separate filter aliquot dedicated to ^{14}C analysis (Sect. 2.2.3), ranged from 1.0 to 11.7 µg C m^{-3}, with a mean of 4.2 ± 2.4 µg C m^{-3} (Table S2). Mean OC and EC concentrations, determined independently by NIOSH 5040 thermal-optical transmittance on a separate quartz filter aliquot, were 3,764 ± 1,995 and 199 ± 126 ng C m^{-3}, respectively (sum = 4.0 µg C m^{-3}, consistent with the sealed-tube TC mean). OC concentrations ranged from 626 to 9,793

https://doi.org/10.5194/egusphere-2026-3338
Preprint. Discussion started: 5 August 2026

ng C m^{-3}, and EC from 60 to 591 ng C m^{-3}, spanning approximately a tenfold range for both species. OC/EC ratios varied from 6.4 to 51.7 (mean 22.6 ± 12.7; Table S2). These consistently high OC/EC ratios (>10) are characteristic of biogenic secondary organic aerosol (SOA) formation and biomass burning emissions, rather than primary fossil fuel combustion, which typically yields OC/EC ratios of 1-5 (Gentner et al., 2012; Mouteva et al., 2017).

On a small number of days, TC slightly exceeded the corresponding routine 24-h mean $PM_{2.5}$ reported by the WBEA continuous monitor at AMS 1. Because TC (sealed-tube combustion) and $PM_{2.5}$ (continuous monitor) are independent measurements made on different sample streams, this discrepancy most plausibly reflects (i) within-day temporal mismatch between the integrated 24-h filter and the continuous monitor, (ii) spatial heterogeneity of plume impacts on the co-located samplers, and (iii) routine measurement uncertainty in both methods at low $PM_{2.5}$ loadings; carbonate carbon was ruled out by acid fumigation (Sect. 2.2.2).

3.2.2 Relationships Among Carbonaceous Aerosol Components, Meteorology, and Trace Gases

Correlation analyses among meteorological variables, trace gases, and carbonaceous aerosol components are summarized in Fig. S4-S6. TC was most strongly correlated with OC ($\rho = 0.89$), consistent with the dominant contribution of OC to total carbon mass throughout the campaign, and with $PM_{2.5}$ ($\rho = 0.78$). Both relationships were consistent between smoke-impacted and smoke-free periods, confirming their robustness across contrasting source conditions (Fig. S4).

TC and OC were both positively correlated with ambient temperature ($\rho = 0.67$ (Fig. S4) and $\rho = 0.76$ (Fig. S5), respectively), a relationship that likely reflects multiple concurrent processes. Temperature-dependent biogenic VOC emissions from the surrounding boreal forest and their photochemical oxidation to SOA are one plausible contributor (Nagalingam et al., 2024; Wang et al., 2024). Warmer temperatures in the AOSR are also associated with southerly and southwesterly air mass transport, which can carry aged anthropogenic aerosol from oil sand mining regions to the north (Bari and Kindzierski, 2015).

EC was strongly correlated with NO_2 ($\rho = 0.77$), $PM_{2.5}$ ($\rho = 0.53$), and SO_2 ($\rho = 0.51$; Fig. S6). Diesel heavy-haul fleets and upgrader and flaring stacks in the AOSR are well-established co-sources of EC, SO_2, and NO_x (Cheng et al., 2020; Gordon et al., 2015; Horb et al., 2021). The late-May pollution episode illustrates how meteorological conditions can amplify local industrial emission signals at AMS 1. On 31 May 2017, concurrent peaks in EC, SO_2, and NO_x (Fig. 2) are consistent with stagnant high-pressure meteorology that suppressed vertical mixing and promoted near-surface accumulation of locally emitted pollutants. Isotopic analysis of the filter sample collected during this period (31 May 2017; $F^{14}C$-TC = 0.37, $F^{14}C$-EC = 0.41) confirmed that fossil-derived carbon accounted for approximately 59-64% of carbonaceous aerosol mass, providing direct isotopic evidence that the concurrent EC-SO_2-NO_x signal reflected fossil fuel combustion from oil sands operations rather than long-range transport or other contemporary sources (see 3.3).

https://doi.org/10.5194/egusphere-2026-3338
Preprint. Discussion started: 5 August 2026

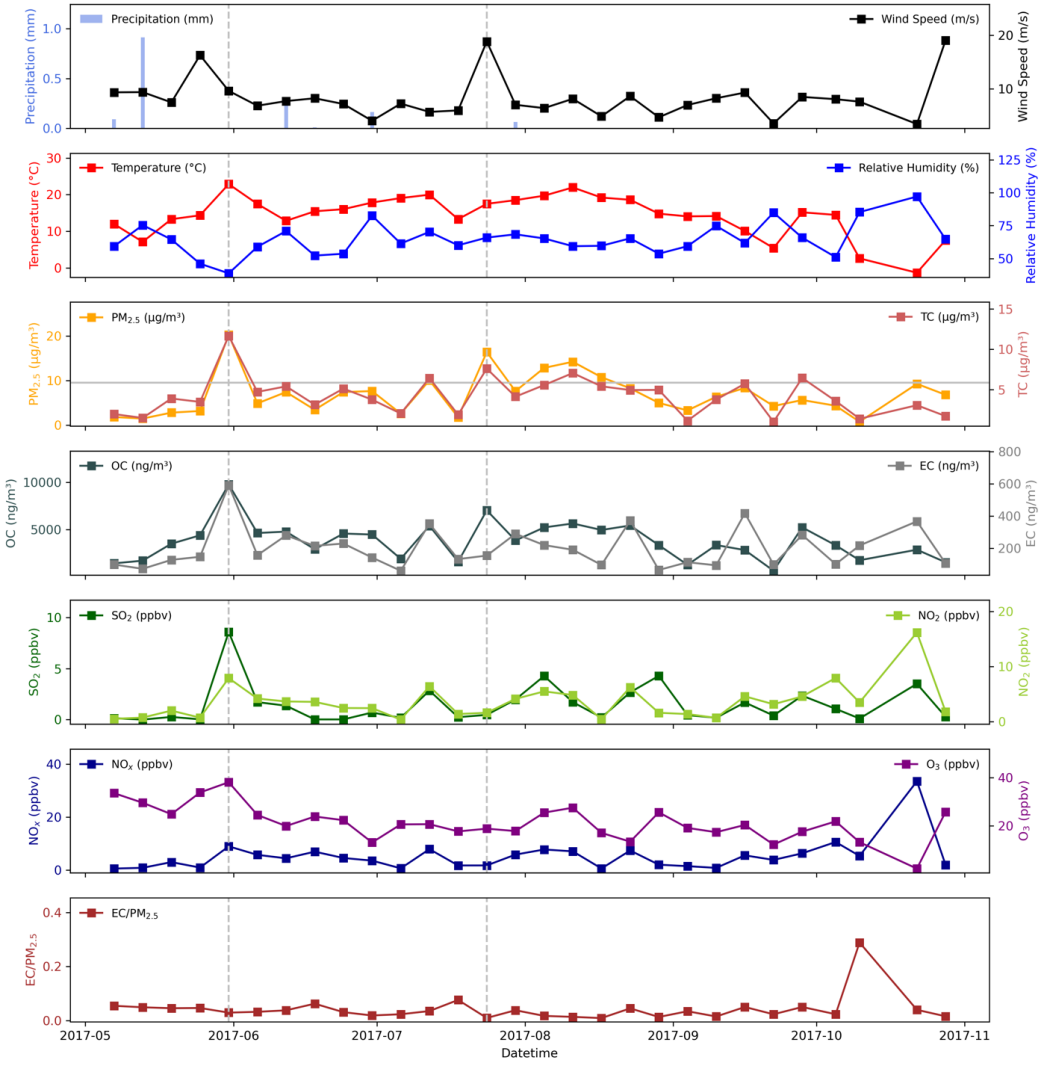

Figure 2. Time series of meteorological parameters and measured air pollutants during the sampling period at AMS 1. Two samples (n = 2) with highest $PM_{2.5}$ concentrations were selected for ^{14}C-EC analysis and are marked with grey dashed lines. The horizontal grey solid line in panel 3 represents the "Moderate" AQI threshold.

3.2.3 Sources of $PM_{2.5}$ Aerosol

$F^{14}C$ values of TC (Fig. 3; Table S3) exhibited substantial temporal variability during the study period, ranging from 0.22 to 1.00, spanning from fossil fuel-dominated to modern biogenic or biomass burning sources. This variability was strongly linked to air mass origin and wildfire activity.

Based on HYSPLIT 10-day back-trajectory cluster analysis, sampling periods were classified into three transport regimes: westerly (n = 14, 48%), northerly (n = 8, 28%), and mixed (n = 7, 24%). Periods were assigned as northerly when northerly flow accounted for more than 60% of cluster distribution, and as westerly when westerly flow exceeded the same threshold; periods in which northerly, westerly, and other directional components each contributed comparable proportions were classified as mixed. Westerly

https://doi.org/10.5194/egusphere-2026-3338
Preprint. Discussion started: 5 August 2026

air masses, which traversed active oil sands mining and upgrading areas to the west and southwest of AMS 1, were more ^{14}C-depleted ($F^{14}C = 0.58 \pm 0.22$) than northerly air masses ($F^{14}C = 0.63 \pm 0.14$), which originated from the Arctic and boreal interior with fewer industrial emission sources, yielding relatively enriched ^{14}C signatures consistent with greater contemporary carbon contributions.

Wildfire smoke, identified using the NOAA HMS Fire and Smoke Product, affected 59% of the sampling period. Smoke-impacted periods were concentrated in July-September 2017, during which $F^{14}C$ of TC was dominated by contemporary carbon attributable to biomass burning from Canada's boreal forest region (Fig. 3; Fig. 4e). The dual-isotope Monte Carlo (MC) source apportionment indicated that biomass burning (f_{bb}) accounted for an average of 45% of TC (range: 9-76%), contemporary biogenic SOA (f_c) contributed an average of 27% (range: 15-32%), and fossil fuel emissions averaged 28% (range: 9-58%). A sensitivity test in which the fossil-fuel $\delta^{13}C$ endmember was shifted from −24.9 ± 3.1‰ (Martinsson et al., 2017) to a bitumen-weighted value of −28 ± 2‰ left f_{ff} values within ±5% for samples with $\delta^{13}C$ between −25 and −28‰, but yielded no valid solutions for samples with $\delta^{13}C \geq -24$‰. This indicates that the most ^{13}C-enriched fossil-dominated samples (e.g., 29 August 2017, $\delta^{13}C = -19.3$‰) cannot be explained by a parent-bitumen fossil endmember and require an isotopically enriched fossil source consistent with photochemical aging or biodegradation (see Section 3.3.1).

In contrast, during smoke-free periods, concentrated in May-June and October 2017, fossil fuel contributions were substantially elevated, averaging 51% of TC (range: 26-77%). These results demonstrate a clear seasonal partitioning of TC sources: fossil fuel combustion from oil sands operations dominated during non-fire periods, while wildfire biomass burning temporarily superseded fossil contributions during the peak summer fire season. This seasonal dynamic underscores the dual anthropogenic-natural forcing of air quality in the AOSR and highlights the importance of accounting for wildfire activity when interpreting $PM_{2.5}$ trends in this industrially impacted region.

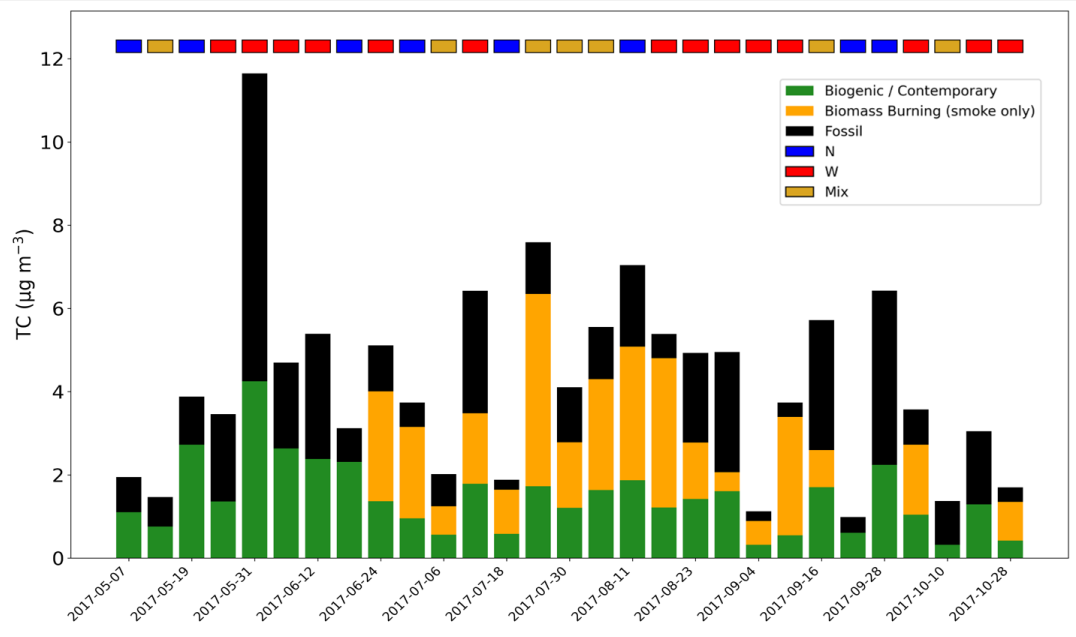

Figure 3. Temporal distribution and isotopic source apportionment of total carbon (TC, µg m^{-3}) for all samples. Stacked bars represent apportioned TC contributions from (1) smoke-free periods using two-source isotopic mass balance: fossil fuel combustion (black), contemporary emissions (green); (2) smoke-impacted periods using three sources MC simulation with $\delta^{13}C$and $F^{14}C$ constraints: fossil fuel

https://doi.org/10.5194/egusphere-2026-3338
Preprint. Discussion started: 5 August 2026

combustion (black), biogenic emissions (green), and biomass burning (yellow). The color bar at the top indicates the dominant air mass back-trajectory cluster for each sampling period.

Given that most filter samples contained insufficient EC carbon mass for ^{14}C analysis, EC ^{14}C measurements were performed on the two samples with the highest TC loading (31 May and 24 July 2017), representing contrasting source conditions (Table S3; Fig. 3).

On 31 May 2017, both TC and EC were strongly fossil-dominated ($F^{14}C$-TC = 0.37, $F^{14}C$-EC = 0.41; Table S3), yielding fossil fuel fractions of 64% and 59% for TC and EC, respectively. The close agreement between $F^{14}C$-TC and $F^{14}C$-EC on this date is consistent with fossil combustion sources driving both OC and EC variability, likely from diesel heavy-haul fleet emissions and upgrader stack sources under stagnant atmospheric conditions. This interpretation is supported by peak SO_2 and NO_x concentrations and limited atmospheric mixing inferred from the meteorological record (Fig. 2). The OC/EC ratio on this date reflects a relatively higher EC contribution relative to OC compared to other sampling periods, consistent with dominant fresh fossil combustion emissions during this episode.

On 24 July 2017, a day with documented wildfire smoke influence, both TC and EC were dominated by contemporary carbon ($F^{14}C$-TC = 0.79, $F^{14}C$-EC = 0.70). Three-source MC apportionment of TC yielded biomass-burning, biogenic-SOA, and fossil contributions of 61%, 23%, and 16%, respectively (84% total contemporary; Table S3, S4). EC was apportioned with a two-source biomass-burning–vs.–fossil mass balance, giving f_{bb}-EC = 70% and f_{ff}-EC = 30% (Table S3, S4). The markedly elevated OC/EC ratio (45.7) on this date was consistent with the substantial contribution of OC-rich biomass burning emissions and the secondary organic aerosol typically associated with wildfire plumes (Landis et al., 2018; Mouteva et al., 2015a, b). The elevated $F^{14}C$-EC specifically confirmed that even the light-absorbing, combustion-derived carbon fraction was primarily fire-derived rather than fossil, reinforcing that wildfire events can temporarily overwhelm the background fossil fuel signal at AMS 1.

Despite the large contrast between these two dates, the fossil fuel signal remained detectable even during the July 24 smoke event (fossil fraction: about 16% of TC), suggesting that oil sands operations maintain a persistent and measurable imprint on carbonaceous aerosol in the AOSR even when wildfire emissions are elevated. This is consistent with the proximity of AMS 1 to active surface mining and upgrading facilities and with the continuous nature of oil sands emissions regardless of season. The close agreement between $F^{14}C$-TC and $F^{14}C$-EC across both dates suggests that EC may serve as a useful first-order proxy for the fossil/contemporary partitioning of TC in this environment when TC and EC share common dominant sources, as is the case under both fossil-dominated (oil sands) and biomass-dominated (wildfire) conditions. However, this proxy relationship has a clear limitation: in periods dominated by biogenic SOA from boreal vegetation, or by fossil-derived secondary organic aerosol from VOC oxidation, TC will carry a substantially different $F^{14}C$ signature from EC because these secondary OC sources have no direct EC counterpart. Under such conditions, EC-based constraints on TC source apportionment will systematically underestimate the contemporary biogenic contribution to total carbon mass.

The agreement between $F^{14}C$-TC and $F^{14}C$-EC across these two contrasting periods raises the possibility that TC ^{14}C measurements may provide a first-order constraint on source apportionment in cases where EC-specific ^{14}C measurements are unavailable. However, this inference must be treated with considerable caution: it is based on only two 24 h samples, both selected specifically for their high TC loading and therefore not representative of background conditions. Furthermore, the moderate overall correlation between OC and EC concentrations across all samples ($\rho = 0.52$, $R^2 = 0.27$) indicates that approximately 73% of EC variability cannot be explained by TC or OC alone, reflecting additional source-specific controls on EC that would decouple $F^{14}C$-TC and

https://doi.org/10.5194/egusphere-2026-3338
Preprint. Discussion started: 5 August 2026

$F^{14}C$-EC under other conditions. In particular, this proxy relationship would break down in periods dominated by biogenic secondary organic aerosol, which contributes to OC and TC but not to EC, or by fossil secondary organic aerosol, both of which would shift $F^{14}C$-TC away from $F^{14}C$-EC without any change in primary emission sources.

3.3 Comparison with Other Arctic and Boreal Regions

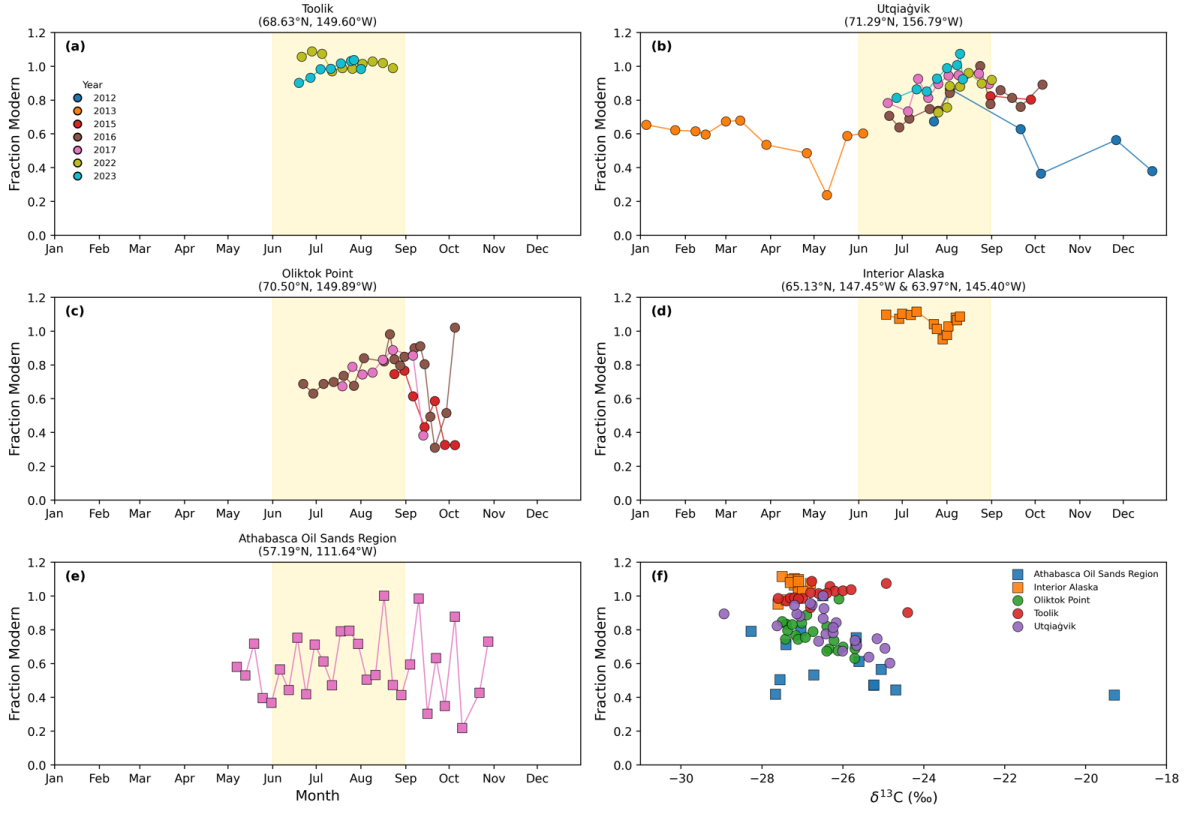

Figure 4. Comparison of ^{14}C and $\delta^{13}C$ signatures of carbonaceous aerosols across Arctic and boreal sites. Panels a-e: Time series of $F^{14}C$ values at individual sites: (a) Toolik Field Station, AK, (b) Utqiaġvik, AK, (c) Oliktok Point, AK, (d) Interior Alaska (Caribou Creek and Delta Junction, AK), and (e) Athabasca Oil Sands Region, Alberta (this study). The yellow shading denotes the summer period (June-August, JJA). Symbol colours indicate sampling year as shown in the legend in panel (a). Panel (f): Scatter plot of $F^{14}C$ versus $\delta^{13}C$ of aerosol samples from all sites (JJA). Symbol colors represent sites, while marker shapes indicate aerosol size fractions (circles: TSP; squares: $PM_{2.5}$).

The isotopic composition of carbonaceous aerosol in the AOSR, shaped by a persistent local fossil fuel source overlaid with variable contemporary contributions, raises the question of how this source regime compares to other sites across the North American boreal and Arctic region. To address this, we compared the isotopic composition of carbonaceous aerosols measured in this study with previously reported data from several Arctic and boreal sites, including Toolik Field Station (Welch et al., 2025), Utqiaġvik (Barrett and Sheesley, 2017; Moffett et al., 2022; Welch et al., 2025), Caribou Creek and Delta Junction (Mouteva et al., 2015b), and Oliktok Point (Moffett et al., 2022) (Fig. 4).

Across most Arctic interior sites (Toolik, Caribou Creek, Delta Junction), $F^{14}C$ values cluster near unity ($F^{14}C \approx 0.9$-1.1) during the summertime (June-August, JJA), indicating that carbonaceous aerosols are dominated by contemporary carbon sources. The corresponding $\delta^{13}C$ signatures at these sites fall largely within the range typical of C3 plant-derived carbon (approximately -27‰

https://doi.org/10.5194/egusphere-2026-3338
Preprint. Discussion started: 5 August 2026

to -25‰), consistent with contributions from biogenic secondary organic aerosol and biomass burning in boreal ecosystems (Moffett et al., 2022; Welch et al., 2025). Outside the summer period, $F^{14}C$ values at these interior sites decline modestly, reflecting reduced biogenic activity and the diminishing wildfire contribution.

In contrast, AOSR measurements displayed substantially lower and more variable $F^{14}C$ values (range: 0.21-1.04). Even during the peak fire season (JJA), when wildfire smoke temporarily elevated $F^{14}C$ toward contemporary values, mean $F^{14}C$ (0.61 ± 0.17; JJA) remained substantially lower than summertime values at any of the Alaskan comparison sites. This persistent signature of $F^{14}C$ indicates a substantial contribution from fossil carbon sources associated with oil sands extraction, upgrading operations, and associated transportation fleets. The observed variability reflects the combined influence of local industrial emissions and episodic wildfire smoke transport.

Measurements from Utqiaġvik and Oliktok Point showed a wider range of $F^{14}C$ values that partially overlapped with those observed in the AOSR, particularly during non-summer months. At these Arctic coastal locations, several samples exhibited relatively depleted radiocarbon signatures ($F^{14}C \approx 0.3$-0.7). This pattern suggests that fossil carbon signals at coastal Arctic sites are most apparent when contemporary carbon sources are seasonally suppressed, a dynamic that contrasts with the AOSR where fossil signals persist year-round regardless of season. The fossil carbon influence at Utqiaġvik and Oliktok Point likely reflects a combination of regional oil and gas activities on Alaska's North Slope, including aerosol transport from Prudhoe Bay facilities (Barrett and Sheesley, 2017; Gunsch et al., 2017), long-range transport of fossil fuel combustion products, and marine shipping emissions from the Arctic Ocean (Welch et al., 2025; Winiger et al., 2019). Atmospheric ageing and secondary aerosol formation during long-range transport may further modify isotopic signatures, contributing to the broader spread in $\delta^{13}C$ (especially $\delta^{13}C > -24$‰) and $F^{14}C$ values observed at these coastal sites (Dasari et al., 2019; Kawamura et al., 2026; Morera-Gómez et al., 2021).

Taken together, these comparisons reveal a clear gradient in fossil carbon influence among the North American Arctic and boreal sites compared to AOSR (Fig. 4f). Remote boreal and Arctic interior sites (Toolik, Caribou Creek, Delta Junction) exhibited the lowest fossil carbon contributions, with summertime $F^{14}C$ values consistently near or above unity, indicating that contemporary biogenic and biomass burning sources account for nearly all carbonaceous aerosol mass during the warm season. Coastal Alaskan sites (Utqiaġvik, Oliktok Point) occupied an intermediate position, with most $F^{14}C$ values in the contemporary range but episodic excursions to lower values ($F^{14}C \approx 0.3$-0.7) during non-summer months, reflecting intermittent fossil carbon inputs from long-range transport and regional North Slope oil and gas activities. Among all sites compared here, the AOSR ranked highest in fossil carbon influence, even during the fire season. We note that the comparison sites were sampled across different years (2012-2023), and interannual variability in wildfire activity, which strongly modulates summertime $F^{14}C$ at all boreal and Arctic sites, introduces uncertainty into direct cross-site comparisons; nonetheless, the consistently lower AOSR $F^{14}C$ relative to all other sites during analogous non-fire conditions supports the robustness of this gradient. The AOSR thus represents an end-member in the fossil-to-contemporary carbon spectrum among these sites, driven by continuous, high-intensity, proximate industrial combustion from surface mining, bitumen upgrading, and heavy-haul diesel fleets, a source regime with no analogue at the remote North American Arctic and boreal sites included in this comparison. We note that AOSR samples were $PM_{2.5}$ whereas most Arctic comparison records are TSP, which includes coarse-mode carbonaceous material absent from $PM_{2.5}$; comparisons here therefore reflect both site and size-cut differences.

https://doi.org/10.5194/egusphere-2026-3338
Preprint. Discussion started: 5 August 2026

3.3.1 Anomalously enriched $\delta^{13}C$ in fossil-dominated samples

Several fossil-dominated samples exhibited $\delta^{13}C$-TC values (29 August 2017, −19.3‰; 25 May 2017, −20.2‰; 31 May 2017, −22.4‰) that were more enriched than parent Athabasca bitumen (≈ −29.6‰), than gasoline and diesel exhaust compiled in the literature (−24 to −28‰; Widory, 2006), and the biomass-burning and biogenic endmembers used here (~−27.2). Carbonate carbon was excluded by acid fumigation of every filter aliquot prior to combustion (Sect. 2.2.3), and the $PM_{2.5}$ size cut excludes most coarse mineral dust, so the enriched signal must reflect organic carbon. We propose that these samples carry SOA generated by atmospheric oxidation of bitumen-derived VOCs released from tailings ponds and mine-face evaporation, which together represent a major regional VOC source in the AOSR (Small et al., 2015; Liggio et al., 2016). OH oxidation of fossil VOCs imposes a kinetic isotope effect of approximately +5 to +9‰ on residual gas and resulting SOA (Goldstein and Shaw, 2003; Rudolph and Czuba, 2000), which, applied to a bitumen-VOC starting composition near −29‰, yields SOA $\delta^{13}C$ in the −20 to −24‰ range, matching our observations. The sensitivity analysis (Sect. 3.2.3) confirms that these samples cannot be reconciled with a parent-bitumen fossil endmember and require an isotopically processed fossil source. Direct $\delta^{13}C$ measurements of tailings-pond VOC emissions have not, to our knowledge, been reported, and targeted source characterisation would directly test this hypothesis.

4 Conclusions

This study presents the first dual-isotope (^{14}C /$\delta^{13}C$) characterization of fine carbonaceous aerosol in the AOSR, based on weekly $PM_{2.5}$ samples collected at Fort McKay (AMS 1) from May to October 2017. TC and OC correlated positively with ambient temperature (ρ = 0.67 and 0.76), consistent with temperature-driven biogenic SOA, while EC was strongly correlated with NO_2 (ρ = 0.77) and SO_2 (ρ = 0.51), implicating diesel mining fleets and upgrader stacks. Source apportionment revealed a clear seasonal partition: fossil fuel combustion accounted for the majority of TC during smoke-free periods (mean 51%, up to 77%), while contemporary biomass burning dominated during wildfire-impacted periods (mean 45%, up to 76%). Westerly air masses traversing active mining and upgrading areas were more ^{14}C-depleted than northerly air masses ($F^{14}C$ = 0.58 ± 0.22 vs. 0.63 ± 0.14). A subset of fossil-dominated samples exhibited $\delta^{13}C$-TC values (−19 to −22‰) that cannot be reconciled with a parent-bitumen fossil endmember, even when that endmember was shifted to bitumen-weighted values in a sensitivity analysis, and that we interpret as SOA generated by photochemical oxidation of bitumen-derived VOCs released from tailings ponds and mine-face evaporation. No other North American Arctic or boreal site previously characterised by ^{14}C exhibits as persistent a fossil-carbon signal as the AOSR, even during the peak fire season. Closing the remaining source-attribution gaps will require direct isotopic measurement of tailings-pond VOC emissions and the resulting SOA, alongside continued dual-isotope monitoring at AMS 1 as oil-sands production and boreal fire activity intensify.

5 Code, data, or code and data availability

The data is available at dryad: DOI: 10.5061/dryad.98sf7m104

6 Supplement link

The link to the supplement will be included by Copernicus, if applicable.

https://doi.org/10.5194/egusphere-2026-3338
Preprint. Discussion started: 5 August 2026

7 Author contributions

LN performed all laboratory analyses, conducted data analysis and source apportionment, and co-wrote the manuscript. XX conceptualised the study, assisted with and supervised the laboratory work, and commented on the manuscript. EBW was responsible for high-volume sampler and filter transfer between AMS 1 and UCI. JTR conceptualised the study, secured funding, and commented on the manuscript. AMW trained and supervised LN on the HYSPLIT back-trajectory analysis and commented on the manuscript. GDS assisted with and supervised the laboratory work and commented on the manuscript. RJS and CEM contributed previously collected Arctic and boreal comparison-site data and edited the manuscript. CIC conceptualised the study, supervised instrument deployment, contributed to data analysis and laboratory work, and drafted and edited the manuscript. All authors reviewed and approved the final manuscript.

8 Competing interests

The authors declare no conflict of interest.

9 Disclaimer

Copernicus Publications remains neutral with regard to jurisdictional claims made in the text, published maps, institutional affiliations, or any other geographical representation in this paper. While Copernicus Publications makes every effort to include appropriate place names, the final responsibility lies with the authors. Views expressed in the text are those of the authors and do not necessarily reflect the views of the publisher.

10 Acknowledgements

We thank the staff of the WBEA Bertha Ganter-Fort McKay (AMS 1) station for facilitating sample collection, the Kleinman lab at UCI for training in the Sunset NIOSH 5040 method, and the staff of UCI's W.M. Keck Carbon Cycle Accelerator Mass Spectrometry (KCCAMS) facility for support with elemental and isotopic analyses. AI tools (ChatGPT/Claude) were used to improve the readability of author written text.

11 Financial support

This work was funded by NASA ABoVE (#TE2014:NNX15AU56A;80NSSC23K0140) and FireSense Programs (80NSSC24K1317) (to JTR) and fellowships from UCI's Undergraduate Research Opportunities Program and CalSpace (to LN).

12 Review statement

The review statement will be added by Copernicus Publications listing the handling editor as well as all contributing referees according to their status anonymous or identified.

https://doi.org/10.5194/egusphere-2026-3338
Preprint. Discussion started: 5 August 2026

13 References

Arciszewski, T. J., Hazewinkel, R. R. O., and Dubé, M. G.: A critical review of the ecological status of lakes and rivers from Canada's oil sands region, Integrated Environmental Assessment and Management, 18, 361–387, https://doi.org/10.1002/ieam.4524, 2021.

Bari, M. A. and Kindzierski, W. B.: Fifteen-year trends in criteria air pollutants in oil sands communities of Alberta, Canada, Environ. Int., 74, 200–208, https://doi.org/10.1016/j.envint.2014.10.009, 2015.

Bari, M. A. and Kindzierski, W. B.: Ambient fine particulate matter (PM2.5) in Canadian oil sands communities: Levels, sources and potential human health risk, Sci. Total Environ., 595, 828–838, https://doi.org/10.1016/j.scitotenv.2017.04.023, 2017.

Barrett, T. E. and Sheesley, R. J.: Year-round optical properties and source characterization of Arctic organic carbon aerosols on the North Slope Alaska, J. Geophys. Res. Atmos., 122, 9319–9331, https://doi.org/10.1002/2016JD026194, 2017.

Berkowitz, N. and Speight, J. G.: The oil sands of Alberta, Fuel, 54, 138–149, https://doi.org/10.1016/0016-2361(75)90001-0, 1975.

Beverly, R. K., Beaumont, W., Tauz, D., Ormsby, K. M., Von Reden, K. F., Santos, G. M., and Southon, J. R.: The Keck Carbon Cycle AMS Laboratory, University of California, Irvine: Status Report, Radiocarbon, 52, 301–309, https://doi.org/10.1017/S0033822200045343, 2010.

Birch, M. E. and Cary, R. A.: Elemental Carbon-Based Method for Monitoring Occupational Exposures to Particulate Diesel Exhaust, Aerosol Sci. Technol., 25, 221–241, https://doi.org/10.1080/02786829608965393, 1996.

Bond, T. C., Doherty, S. J., Fahey, D. W., Forster, P. M., Berntsen, T., DeAngelo, B. J., Flanner, M. G., Ghan, S., Kärcher, B., Koch, D., Kinne, S., Kondo, Y., Quinn, P. K., Sarofim, M. C., Schultz, M. G., Schulz, M., Venkataraman, C., Zhang, H., Zhang, S., Bellouin, N., Guttikunda, S. K., Hopke, P. K., Jacobson, M. Z., Kaiser, J. W., Klimont, Z., Lohmann, U., Schwarz, J. P., Shindell, D., Storelvmo, T., Warren, S. G., and Zender, C. S.: Bounding the role of black carbon in the climate system: A scientific assessment, J. Geophys. Res. Atmos., 118, 5380–5552, https://doi.org/10.1002/jgrd.50171, 2013.

Canadian Interagency Forest Fire Centre: Canada Report 2017, CIFFC, Winnipeg, Manitoba, Canada, 2018.

Cheng, Y., Li, S.-M., Liggio, J., Gordon, M., Darlington, A., Zheng, Q., Moran, M., Liu, P., and Wolde, M.: Top-Down Determination of Black Carbon Emissions from Oil Sand Facilities in Alberta, Canada Using Aircraft Measurements, Environ. Sci. Technol., 54, 412–418, https://doi.org/10.1021/acs.est.9b05522, 2020.

Dasari, S., Andersson, A., Bikkina, S., Holmstrand, H., Budhavant, K., Satheesh, S., Asmi, E., Kesti, J., Backman, J., Salam, A., Bisht, D. S., Tiwari, S., Hameed, Z., and Gustafsson, Ö.: Photochemical degradation affects the light absorption of water-soluble brown carbon in the South Asian outflow, Sci. Adv., 5, eaau8066, https://doi.org/10.1126/sciadv.aau8066, 2019.

Fang, W., Du, K., Andersson, A., Xing, Z., Cho, C., Kim, S., Deng, J., and Gustafsson, Ö.: Dual-Isotope Constraints on Seasonally Resolved Source Fingerprinting of Black Carbon Aerosols in Sites of the Four Emission Hot Spot Regions of China, J. Geophys. Res. Atmos., 123, https://doi.org/10.1029/2018JD028607, 2018.

Fang, W., Evangeliou, N., Eckhardt, S., Xing, J., Zhang, H., Xiao, H., Zhao, M., and Kim, S.-W.: Increased contribution of biomass burning to haze events in Shanghai since China's clean air actions, Commun. Earth Environ., 4, 310, https://doi.org/10.1038/s43247-023-00979-z, 2023.

Fuzzi, S., Baltensperger, U., Carslaw, K., Decesari, S., Denier Van Der Gon, H., Facchini, M. C., Fowler, D., Koren, I., Langford, B., Lohmann, U., Nemitz, E., Pandis, S., Riipinen, I., Rudich, Y., Schaap, M., Slowik, J. G., Spracklen, D. V., Vignati, E., Wild, M., Williams, M., and Gilardoni, S.: Particulate matter, air quality and climate: lessons learned and future needs, Atmos. Chem. Phys., 15, 8217–8299, https://doi.org/10.5194/acp-15-8217-2015, 2015.

Gentner, D. R., Isaacman, G., Worton, D. R., Chan, A. W. H., Dallmann, T. R., Davis, L., Liu, S., Day, D. A., Russell, L. M., Wilson, K. R., Weber, R., Guha, A., Harley, R. A., and Goldstein, A. H.: Elucidating secondary organic aerosol from diesel and gasoline vehicles through detailed characterization of organic carbon emissions, Proc. Natl. Acad. Sci. U.S.A., 109, 18318–18323, https://doi.org/10.1073/pnas.1212272109, 2012.

https://doi.org/10.5194/egusphere-2026-3338
Preprint. Discussion started: 5 August 2026

Goldstein, A. H. and Shaw, S. L.: Isotopes of Volatile Organic Compounds: An Emerging Approach for Studying Atmospheric Budgets and Chemistry, Chem. Rev., 103, 5025–5048, https://doi.org/10.1021/cr0206566, 2003.

Gordon, M., Li, S.-M., Staebler, R., Darlington, A., Hayden, K., O'Brien, J., and Wolde, M.: Determining air pollutant emission rates based on mass balance using airborne measurement data over the Alberta oil sands operations, Atmos. Meas. Tech., 8, 3745–3765, https://doi.org/10.5194/amt-8-3745-2015, 2015.

Gunsch, M. J., Kirpes, R. M., Kolesar, K. R., Barrett, T. E., China, S., Sheesley, R. J., Laskin, A., Wiedensohler, A., Tuch, T., and Pratt, K. A.: Contributions of transported Prudhoe Bay oil field emissions to the aerosol population in Utqiaġvik, Alaska, Atmos. Chem. Phys., 17, 10879–10892, https://doi.org/10.5194/acp-17-10879-2017, 2017.

He, M., Ditto, J. C., Gardner, L., Machesky, J., Hass-Mitchell, T. N., Chen, C., Khare, P., Sahin, B., Fortner, J. D., Plata, D. L., Drollette, B. D., Hayden, K. L., Wentzell, J. J. B., Mittermeier, R. L., Leithead, A., Lee, P., Darlington, A., Wren, S. N., Zhang, J., Wolde, M., Moussa, S. G., Li, S.-M., Liggio, J., and Gentner, D. R.: Total organic carbon measurements reveal major gaps in petrochemical emissions reporting, Science, 383, 426–432, https://doi.org/10.1126/science.adj6233, 2024.

Hein, F. J.: Heavy Oil and Oil (Tar) Sands in North America: An Overview & Summary of Contributions, Nat. Resour. Res., 15, 67–84, https://doi.org/10.1007/s11053-006-9016-3, 2006.

Horb, E. C., Wentworth, G. R., Makar, P. A., Liggio, J., Hayden, K., Boutzis, E. I., Beausoleil, D. L., Hazewinkel, R. O., Mahaffey, A. C., Sayanda, D., Wyatt, F., and Dubé, M. G.: A decadal synthesis of atmospheric emissions, ambient air quality, and deposition in the oil sands region, Integrated Environmental Assessment and Management, 18, 333–360, https://doi.org/10.1002/ieam.4539, 2021.

Jankowski, N., Schmidl, C., Marr, I. L., Bauer, H., and Puxbaum, H.: Comparison of methods for the quantification of carbonate carbon in atmospheric PM10 aerosol samples, Atmospheric Environment, 42, 8055–8064, https://doi.org/10.1016/j.atmosenv.2008.06.012, 2008.

Jiang, F., Liu, J., Cheng, Z., Ding, P., Xu, Y., Zong, Z., Zhu, S., Zhou, S., Yan, C., Zhang, Z., Zheng, J., Tian, C., Li, J., and Zhang, G.: Dual-carbon isotope constraints on source apportionment of black carbon in the megacity Guangzhou of the Pearl River Delta region, China for 2018 autumn season, Environmental Pollution, 294, 118638, https://doi.org/10.1016/j.envpol.2021.118638, 2022.

Jordaan, S. M.: Land and Water Impacts of Oil Sands Production in Alberta, Environ. Sci. Technol., 46, 3611–3617, https://doi.org/10.1021/es203682m, 2012.

Kawamura, K., Watanabe, T., Kasukabe, H., and Barrie, L. A.: Photochemical Aging of Organic Aerosols Drives the Enhancement of Carbon-13 Isotope Ratios of Oxalic, Malonic, Glyoxylic Acids and Total Carbon During the Arctic Polar Sunrise, J. Geophys. Res. Atmos., 131, e2025JD045420, https://doi.org/10.1029/2025JD045420, 2026.

Landis, M. S., Patrick Pancras, J., Graney, J. R., White, E. M., Edgerton, E. S., Legge, A., and Percy, K. E.: Source apportionment of ambient fine and coarse particulate matter at the Fort McKay community site, in the Athabasca Oil Sands Region, Alberta, Canada, Sci. Total Environ., 584–585, 105–117, https://doi.org/10.1016/j.scitotenv.2017.01.110, 2017.

Landis, M. S., Edgerton, E. S., White, E. M., Wentworth, G. R., Sullivan, A. P., and Dillner, A. M.: The impact of the 2016 Fort McMurray Horse River Wildfire on ambient air pollution levels in the Athabasca Oil Sands Region, Alberta, Canada, Sci. Total Environ., 618, 1665–1676, https://doi.org/10.1016/j.scitotenv.2017.10.008, 2018.

Liggio, J., Li, S.-M., Hayden, K., Taha, Y. M., Stroud, C., Darlington, A., Drollette, B. D., Gordon, M., Lee, P., Liu, P., Leithead, A., Moussa, S. G., Wang, D., O'Brien, J., Mittermeier, R. L., Brook, J. R., Lu, G., Staebler, R. M., Han, Y., Tokarek, T. W., Osthoff, H. D., Makar, P. A., Zhang, J., Plata, D. L., and Gentner, D. R.: Oil sands operations as a large source of secondary organic aerosols, Nature, 534, 91–94, https://doi.org/10.1038/nature17646, 2016.

Liggio, J., Li, S.-M., Staebler, R. M., Hayden, K., Darlington, A., Mittermeier, R. L., O'Brien, J., McLaren, R., Wolde, M., Worthy, D., and Vogel, F.: Measured Canadian oil sands CO2 emissions are higher than estimates made using internationally recommended methods, Nat. Commun., 10, https://doi.org/10.1038/s41467-019-09714-9, 2019.

https://doi.org/10.5194/egusphere-2026-3338
Preprint. Discussion started: 5 August 2026

Martinsson, J., Andersson, A., Sporre, M. K., Friberg, J., Kristensson, A., Swietlicki, E., Olsson, P.-A., and Stenström, K. E.: Evaluation of δ13C in Carbonaceous Aerosol Source Apportionment at a Rural Measurement Site, Aerosol Air Qual. Res., 17, 2081–2094, https://doi.org/10.4209/aaqr.2016.09.0392, 2017.

McGaughy, K., Abraham, T., Bergerson, J. A., and Masnadi, M. S.: Canadian oil sands industry GHG emissions intensity and mitigation potential of some key emerging technologies towards fulfilling its 2050 net-zero commitment, Resources, Conservation and Recycling, 218, 108230, https://doi.org/10.1016/j.resconrec.2025.108230, 2025.

McLinden, C. A., Fioletov, V., Boersma, K. F., Kharol, S. K., Krotkov, N., Lamsal, L., Makar, P. A., Martin, R. V., Veefkind, J. P., and Yang, K.: Improved satellite retrievals of NO_2 and SO_2 over the Canadian oil sands and comparisons with surface measurements, Atmos. Chem. Phys., 14, 3637–3656, https://doi.org/10.5194/acp-14-3637-2014, 2014.

McLinden, C. A., Fioletov, V., Krotkov, N. A., Li, C., Boersma, K. F., and Adams, C.: A Decade of Change in NO_2 and SO_2 over the Canadian Oil Sands As Seen from Space, Environ. Sci. Technol., 50, 331–337, https://doi.org/10.1021/acs.est.5b04985, 2016.

Moffett, C. E., Mehra, M., Barrett, T. E., Gunsch, M. J., Pratt, K. A., and Sheesley, R. J.: Contemporary sources dominate carbonaceous aerosol on the North Slope of Alaska, Sci. Total Environ., 831, 154641, https://doi.org/10.1016/j.scitotenv.2022.154641, 2022.

Morera-Gómez, Y., Cong, Z., and Widory, D.: Carbonaceous Fractions Contents and Carbon Stable Isotope Compositions of Aerosols Collected in the Atmosphere of Montreal (Canada): Seasonality, Sources, and Implications, Front. Environ. Sci., 9, 622521, https://doi.org/10.3389/fenvs.2021.622521, 2021.

Mouteva, G. O., Fahrni, S. M., Santos, G. M., Randerson, J. T., Zhang, Y.-L., Szidat, S., and Czimczik, C. I.: Accuracy and precision of ^{14}C-based source apportionment of organic and elemental carbon in aerosols using the Swiss_4S protocol, Atmos. Meas. Tech., 8, 3729–3743, https://doi.org/10.5194/amt-8-3729-2015, 2015a.

Mouteva, G. O., Czimczik, C. I., Fahrni, S. M., Wiggins, E. B., Rogers, B. M., Veraverbeke, S., Xu, X., Santos, G. M., Henderson, J., Miller, C. E., and Randerson, J. T.: Black carbon aerosol dynamics and isotopic composition in Alaska linked with boreal fire emissions and depth of burn in organic soils, Global Biogeochemical Cycles, 29, 1977–2000, https://doi.org/10.1002/2015GB005247, 2015b.

Mouteva, G. O., Randerson, J. T., Fahrni, S. M., Bush, S. E., Ehleringer, J. R., Xu, X., Santos, G. M., Kuprov, R., Schichtel, B. A., and Czimczik, C. I.: Using radiocarbon to constrain black and organic carbon aerosol sources in Salt Lake City, J. Geophys. Res. Atmos., 122, 9843–9857, https://doi.org/10.1002/2017JD026519, 2017.

Nagalingam, S., Wang, H., Kim, S., and Guenther, A.: Unexpectedly strong heat stress induction of monoterpene, methylbutenol, and other volatile emissions for conifers in the cypress family (Cupressaceae), Sci. Total Environ., 956, 177336, https://doi.org/10.1016/j.scitotenv.2024.177336, 2024.

Oil Sands Monitoring Program: Annual Report for 2024-25, Alberta Environment and Protected Areas, Government of Alberta, Edmonton, Alberta, Canada, ISBN 9781460163894, 2025.

Phillips-Smith, C., Jeong, C.-H., Healy, R. M., Dabek-Zlotorzynska, E., Celo, V., Brook, J. R., and Evans, G.: Sources of particulate matter components in the Athabasca oil sands region: investigation through a comparison of trace element measurement methodologies, Atmos. Chem. Phys., 17, 9435–9449, https://doi.org/10.5194/acp-17-9435-2017, 2017.

Rolph, G., Stein, A., and Stunder, B.: Real-time Environmental Applications and Display sYstem: READY, Environmental Modelling & Software, 95, 210–228, https://doi.org/10.1016/j.envsoft.2017.06.025, 2017.

Rosa, L., Davis, K. F., Rulli, M. C., and D'Odorico, P.: Environmental consequences of oil production from oil sands, Earth's Future, 5, 158–170, https://doi.org/10.1002/2016ef000484, 2017.

Rudolph, J. and Czuba, E.: On the use of isotopic composition measurements of volatile organic compounds to determine the "photochemical age" of an air mass, Geophys. Res. Lett., 27, 3865–3868, https://doi.org/10.1029/2000GL011477, 2000.

Scholten, R. C., Veraverbeke, S., Chen, Y., and Randerson, J. T.: Spatial variability in Arctic–boreal fire regimes influenced by environmental and human factors, Nat. Geosci., 17, 866–873, https://doi.org/10.1038/s41561-024-01505-2, 2024.

https://doi.org/10.5194/egusphere-2026-3338
Preprint. Discussion started: 5 August 2026

Small, C. C., Cho, S., Hashisho, Z., and Ulrich, A. C.: Emissions from oil sands tailings ponds: Review of tailings pond parameters and emission estimates, J. Pet. Sci. Eng., 127, 490–501, https://doi.org/10.1016/j.petrol.2014.11.020, 2015.

Spracklen, D. V., Bonn, B., and Carslaw, K. S.: Boreal forests, aerosols and the impacts on clouds and climate, Phil. Trans. R. Soc. A., 366, 4613–4626, https://doi.org/10.1098/rsta.2008.0201, 2008.

Stein, A. F., Draxler, R. R., Rolph, G. D., Stunder, B. J. B., Cohen, M. D., and Ngan, F.: NOAA's HYSPLIT Atmospheric Transport and Dispersion Modeling System, Bulletin of the American Meteorological Society, 96, 2059–2077, https://doi.org/10.1175/BAMS-D-14-00110.1, 2015.

Walker, B. D. and Xu, X.: An improved method for the sealed-tube zinc graphitization of microgram carbon samples and ^{14}C AMS measurement, Nuclear Instruments and Methods in Physics Research Section B: Beam Interactions with Materials and Atoms, 438, 58–65, https://doi.org/10.1016/j.nimb.2018.08.004, 2019.

Wang, D., Wang, D., Tan, X., Yeung, A., and Liu, Q.: A review of the roles of constituent minerals and residual bitumen in the solid-liquid separation of oil sands tailings, Journal of Hazardous Materials, 451, 131178, https://doi.org/10.1016/j.jhazmat.2023.131178, 2023.

Wang, H., Nagalingam, S., Welch, A. M., Leong, C., Czimczik, C. I., and Guenther, A. B.: Heat waves may trigger unexpected surge in aerosol and ozone precursor emissions from sedges in urban landscapes, Proc. Natl. Acad. Sci. U.S.A., 121, e2412817121, https://doi.org/10.1073/pnas.2412817121, 2024.

Welch, A. M., Matthews, T., Sheesley, R. J., Wang, H., Barsanti, K. C., Nielsen, N., Xu, X., Niu, L., Guenther, A. B., and Czimczik, C. I.: Summertime Carbonaceous Aerosol in Interior Versus Coastal Northern Alaska, J. Geophys. Res. Atmos., 130, https://doi.org/10.1029/2024jd042080, 2025.

Widory, D.: Combustibles, fuels and their combustion products: A view through carbon isotopes, Combust. Theor. Model., 10, 831–841, https://doi.org/10.1080/13647830600720264, 2006.

Winiger, P., Andersson, A., Eckhardt, S., Stohl, A., Semiletov, I. P., Dudarev, O. V., Charkin, A., Shakhova, N., Klimont, Z., Heyes, C., and Gustafsson, Ö.: Siberian Arctic black carbon sources constrained by model and observation, Proc. Natl. Acad. Sci. U.S.A., 114, https://doi.org/10.1073/pnas.1613401114, 2017.

Winiger, P., Barrett, T. E., Sheesley, R. J., Huang, L., Sharma, S., Barrie, L. A., Yttri, K. E., Evangeliou, N., Eckhardt, S., Stohl, A., Klimont, Z., Heyes, C., Semiletov, I. P., Dudarev, O. V., Charkin, A., Shakhova, N., Holmstrand, H., Andersson, A., and Gustafsson, Ö.: Source apportionment of circum-Arctic atmospheric black carbon from isotopes and modeling, Sci. Adv., 5, https://doi.org/10.1126/sciadv.aau8052, 2019.

Xing, Z., Xiong, Y., and Du, K.: Source apportionment of airborne particulate matters over the Athabasca oil sands region: Inter-comparison between PMF modeling and ground-based remote sensing, Atmospheric Environment, 221, 117103, https://doi.org/10.1016/j.atmosenv.2019.117103, 2020.

Xu, X., Trumbore, S. E., Zheng, S., Southon, J. R., McDuffee, K. E., Luttgen, M., and Liu, J. C.: Modifying a sealed tube zinc reduction method for preparation of AMS graphite targets: Reducing background and attaining high precision, Nuclear Instruments and Methods in Physics Research Section B: Beam Interactions with Materials and Atoms, 259, 320–329, https://doi.org/10.1016/j.nimb.2007.01.175, 2007.

You, Y., O'Brien, J. M., Cole, A. S., Zhang, L., He, Z., Feng, J., and Pearson, S.: Contribution of emissions from the oil sands activities in Alberta, Canada to atmospheric concentration and deposition of nitrogen and sulfur species at a downwind site, Environmental Pollution, 356, 124301, https://doi.org/10.1016/j.envpol.2024.124301, 2024.

Zhang, Q., Shen, Z., Cao, J., Zhang, R., Zhang, L., Huang, R.-J., Zheng, C., Wang, L., Liu, S., Xu, H., Zheng, C., and Liu, P.: Variations in PM2.5, TSP, BC, and trace gases (NO2, SO2, and O3) between haze and non-haze episodes in winter over Xi'an, China, Atmospheric Environment, 112, 64–71, https://doi.org/10.1016/j.atmosenv.2015.04.033, 2015.